Comprehensive Design Space Exploration of Silicon Photonic Interconnects

Meisam Bahadori, *Student Member, IEEE*, Sébastien Rumley, *Member, IEEE*, Dessislava Nikolova, and Keren Bergman, *Fellow, IEEE, Fellow, OSA*

***Abstract*—The paper presents a comprehensive physical layer design and modeling platform for silicon photonic interconnects. The platform is based on explicit closed-form expressions for optical power penalties, derived for both signal-dependent and signal-independent noise contexts. Our models agree well with reported experimental measurements. We show how the modeling approach is used for the design space exploration of silicon photonic links and can be leveraged to optimize the wavelength-division multiplexed (WDM) capacity, evaluate the scalability, and study the sensitivity of the system to key device parameters. We apply the methodology to the design of microring-based silicon photonic links, including an evaluation of the impairments associated with cascaded ring modulators, as well as the spectral distortion and crosstalk effects of demultiplexer ring arrays for nonreturn-to-zero (NRZ) ON–OFF keying (OOK) modulated WDM signals. We show that the total capacity of a chip-to-chip microring-based WDM silicon photonic link designed with recently reported interconnect device parameters can approach 2 Tb/s realized with NRZ-OOK data modulation and 45 wavelengths each modulated at 45 Gb/s.**

***Index Terms*—Microring resonators, optical interconnects, silicon photonics.**

I. Introduction

With the vast rise in parallel multicore architectures, the scalability of computing performance is increasingly reliant on the availability of high-bandwidth, energy efficient data communications infrastructure. Silicon photonics has attracted considerable interest [1]–[3] as an emerging technology that can offer close integration of CMOS electronics with optical devices [4], [5]. This technology has the potential for delivering ultra high bandwidth interconnect solutions that are at the same time energy efficient and available at low cost. Silicon photonics has been proposed for designing efficient networks-on-chip [6]–[10], for supporting global interconnects for datacenters [11], and high performance computing systems [12], [13]. It has been also presented as an enabling technology for realizing Exascale computing systems (i.e., Supercomputers capable of realizing 10^{18} operations per second) [14], [15]. The chip-scale integration of electronics and photonics may further alleviate the limitations of electronic chips in terms of I/O pin count [16], [17].

Although multiple experimental demonstrations of silicon photonic devices, sub-systems or systems [18]–[21] have been reported in the last decade, the technology is still young and only recently emerging for commercial systems adoption. Significant design space exploration is required to understand the performance and impact of silicon photonics for computing interconnects. The design methodology for implementing electro-optical interfaces at the transmitters and receivers must be developed. In particular, it is critical to understand how silicon photonic optical modulators, multiplexers, and demultiplexers can be combined to obtain optimized, thus efficient, WDM links.

In this paper, we present a uniquely comprehensive modeling platform for efficiently exploring the design space of silicon photonic interconnects, from the physical layer to the link-level analysis. We concentrate our efforts on microring-resonator (MRR)-based links, as they offer the highest bandwidth density and most energy efficient performance among current silicon photonic interconnect devices [22]–[24]. MRRs can be designed to perform several interconnect functions and represent the key building blocks of silicon photonic systems [25], [26]. MRRs can be used both as active modulators and switches, as well as wavelength-selective passive filters. When acting as modulators [27]–[33], they leverage plasma dispersion effects of silicon [34]–[36] which provides an efficient way of changing the effective refractive index of the ring by injecting or depleting charge carriers. Such modulation scheme has proven to be capable of delivering high-speed modulations, e.g., 10 Gb/s or higher with low energy consumption [22], [24], [37]–[41]. When used as demultiplexers, a ring operates as a passive drop filter whose resonance is tuned to a specific channel wavelength [23], [42], [43]. In this case, fine-tuning is carried out via integrated heaters that are implemented on top of the silicon microring [44], [45]. First order or higher order add-drop filters have been fabricated and demonstrated in recent years [46], [47]. MRRs are generally very sensitive to thermal fluctuations [48], [49], but several stabilization mechanisms (e.g., wavelength-locking schemes) have been proposed in recent years to redress this vulnerability [50]–[55]. MRRs can also switch multiple wavelengths from one waveguide to another and spatially route them to another path [56]–[60].

Due to their small size, many microrings can be cascaded on a single on-chip bus waveguide, facilitating the dense wavelength-division-multiplexing design and operation of the link [61]–[63]. However, WDM links may suffer from spectral

Manuscript received July 22, 2015; revised October 4, 2015; accepted November 16, 2015. Date of publication November 22, 2015; date of current version June 1, 2016. This work was supported by DARPA Microsystems Technology Office under the Computing With Optically Enabled Data Movement Project and the Power Efficiency Revolution for Embedded Computing Technologies Program, by the U.S. Department of Energy, National Nuclear Security Administration, Advanced Simulation and Computing program under Contract PO1426332 with Sandia National Laboratories, and by Freedom Photonics, Inc.

The authors are with the Department of Electrical Engineering, Columbia University, New York, NY 10027 USA (e-mail: mb3875@columbia.edu; sr3061@columbia.edu; dnn2108@columbia.edu; kb2028@columbia.edu).

Color versions of one or more of the figures in this paper are available online at http://ieeexplore.ieee.org.

Digital Object Identifier 10.1109/JLT.2015.2503120

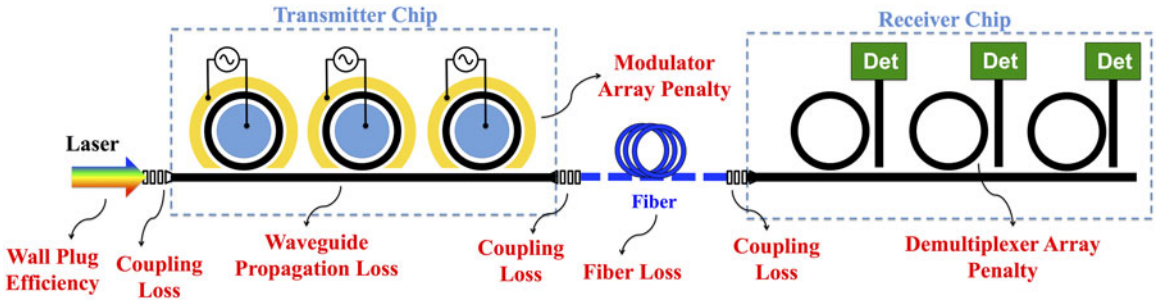

Fig. 1. Chip-to-Chip silicon photonic interconnect with an MRR-based WDM link. The optical interface of the transmitter chip includes MRR modulators that act upon carrier dispersion principle for high speed modulation. The optical interface at the receiver includes Demux filters, photodetectors, and electronic decision circuitry (Det: detector). Wall-plug efficiency corresponds to the electrical to optical power conversion of the laser.

degradationof channels and inter-channel crosstalk [64]–[72]. These impairments eventually put an upper limit on both the modulation speed of each channel and on the number of channels, thus placing an upper bound on the maximum aggregate rate of the link [73], [74].

In this paper, we present the design and modeling platform for obtaining the maximum achievable aggregate bandwidth in a short-distance silicon photonic link with microring modulators and filters. This is achieved by estimating the effects of the induced impairments and translating them into power penalties, i.e., an amount of extra optical power that permits compensation for the effects of such impairments on the bit-error-ratio (BER) performance of the system [75]–[79]. We also show how the spectral statistics of a modulated light changes when it goes through a ring demultiplexer and how that can be turned into power penalty.

The rest of this paper is organized as follows: in Section II, we set forth our approach in analyzing the optical power budget of a silicon photonic link and provide a brief review of the most important characteristics of non-return-to-zero ON–OFF keying (NRZ-OOK) modulation and estimation of BER-associated power penalties. The analysis is based on how the statistics of the optical signal changes as it undergoes modulation and filtering. Sections III and IV provide details of the power penalties associated with ring modulators and demultiplexers. Several available experimental measurements of power penalties are presented to back-up theoretical estimations. In Section V, we present our discussion of optimizing the ring parameters in order to achieve minimum power penalty throughout the MRR-based link. In Section VI, the link analysis is given for a realistic power budget. Finally, conclusion is drawn in Section VII. Two appendices are also provided with details of obtaining equations presented in the paper for microring demultiplexers.

II. Description of the Approach

A. Optical Power Budget and Power Penalties

Consider a simple chip-to-chip silicon photonic link as shown in Fig. 1. On the transmitter side, cascaded microrings along an on-chip waveguide modulate the incoming multi-wavelength light generated by a comb laser source [80]. The incoming wavelengths, once imprinted with data, are then transmitted through an optical fiber to a receiver chip. The receiver chip consists of multiple passive microrings whose resonances are tuned to channel wavelengths. The total capacity of this link is obtained by multiplying the number of channels (wavelengths) with the modulation bit rate. Intuitively, it is tempting to maximize the number of wavelengths, and/or to choose higher bit rates for each channel. This allows for higher utilization of the available spectrum in the transmission media. However, as either the number of wavelengths and/or the bit rate grows, crosstalk and other undesired impairments emerge and eventually prevent reliable transmission. The total capacity of the link is closely tied to the optical power losses and impairments that the light experiences over the entire link. Summing up all the power penalties of the link, $\mathrm{PP}^{\mathrm{dB}}$, for a single channel, the following inequality must hold [81]:

$$\left[\mathrm{P}^{\mathrm{dBm}}_{\mathrm{laser}} - 10\log_{10}(N_\lambda)\right] - \mathrm{P}^{\mathrm{dBm}}_{\mathrm{sensitivity}} \geq \mathrm{PP}^{\mathrm{dB}}_{\mathrm{tot}}. \tag{1}$$

In general, aggregated optical power $\mathrm{P}_{\mathrm{laser}}$ (sum over all wavelengths) must stay below the nonlinear threshold of the silicon waveguides at any point of the link [70], [74]. In contrast, the signal powers should stay above the sensitivity of the detectors $\mathrm{P}_{\mathrm{sensitivity}}$ (minimum number of photons or equivalently a certain amount of optical power) at the receive side. A typical receiver may have a sensitivity of -12.7 dBm at 8 Gb/s operation [77], while a good receiver may exhibit a sensitivity of about -21 dBm at 10 Gb/s [75]. The difference between lower and higher thresholds results in the maximum power budget that can be exploited. This budget accounts for the power penalty per channel (how much higher should the signal hit the detector) $\mathrm{PP}_{\mathrm{tot}}$, and for the product over the N_λ channels. We will show that the power impairments induced by the rings depend on the spacing between channels, which is inversely proportional to the number of wavelengths, and on the modulation rate r_b. Eq. (1) is therefore a nonlinear function of N_λ and r_b, and determination of the $N_\lambda \times r_b$ product that maximizes the bandwidth directly from it is intractable. It is however possible to optimize the link, i.e., optimize its constituting devices, such that $\mathrm{PP}_{\mathrm{tot}}$ is minimized for different (N_λ , r_b) combinations. We proceed to do this optimization for NRZ-OOK modulation format.

B. Properties of the NRZ-OOK Modulation Format

In an NRZ-OOK modulation, the electrical signal is a sequence of logical 0's and 1's that are imprinted on the envelope of the light. Therefore, the envelope electric field of the modulated

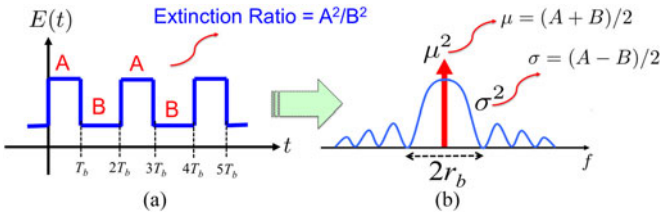

Fig. 2. Envelope electric field of the (a) NRZ-OOK modulation, and its (b) power spectral density. ER is the ratio of the optical power of the high level to the optical power of the low level of the electric field.

light has a form of

$$E(t) = \sum_{k=-\infty}^{\infty} a_k \; p(t - kT_b) \tag{2}$$

where T_b is the bit interval and its inverse ($r_b = 1/T_b$) is the bit rate of the modulation, a_k is the amplitude for 0's and 1's bits, and $p(t)$ is the ideal square pulse of unit amplitude and duration T_b. A picture of such envelope is shown in Fig. 2(a), where the high level is denoted by A and the low level is denoted by B. Ideally, if the modulation has an infinite extinction ratio (ER), then the low level must be zero ($B = 0$); however, in practice ring modulators produce a limited ER. Typical numbers for 10 G devices are 8–10 dB of extinction [24]. It is a practical assumption that all bits are equiprobable and the source of information that generates these bits is a stationary ergodic source. Therefore *Prob*$(a_k = A) = 0.5$ and *Prob*$(a_k = B) = 0.5$.

The average behavior, i.e., statistics, of such modulation is given by the autocorrelation of the envelope electric field over time. The average power spectral density of the envelope of modulation is then the Fourier transform of its autocorrelation, which simplifies to the following equation [82], [83]:

$$S_E(f) = \mu^2 \, \delta(f - f_c) + \sigma^2 \frac{1}{r_b} \text{sinc}^2((f - f_c)/r_b), \tag{3}$$

where

$$\mu = \frac{A + B}{2}, \tag{4a}$$

$$\sigma = \frac{A - B}{2} \tag{4b}$$

f_c is the optical frequency of the light, and $\delta(f - f_c)$ is the Dirac delta function centered at carrier frequency f_c. A plot of this spectrum is presented in Fig. 2(b). The power of the modulated signal is given by integrating Eq. (3) over all frequencies, yielding $\text{P}_{\text{av}} = \mu^2 + \sigma^2$. We note that the power of the NRZ-OOK modulation can be decomposed based on the mean and variance of the envelope electric field. The μ^2 power is at the center frequency (represented by the delta function) and the power of the variance (σ^2) is spread over a spectrum of frequencies (represented by the *sinc* function). We will leverage Eq. (3) to estimate the power penalty of each optical component along the link.

C. Power Penalty Evaluation Based on Signal Statistics

As the modulated light goes through the waveguides, transmission medium, and other optical devices, the quality of the signal degrades. To evaluate the breadth of the degradation, one approach consists of evaluating the new high and low levels (assumed to be A' and B') when the light reaches the receiver. Alternatively, one can analyze how the power spectral density experiences distortion due to the non-ideal frequency response of the link. In other terms, one can evaluate how μ and σ evolve into μ' and σ'. Once these latter values are known, the power penalty associated with the distortion can be derived using one of the two following models widely used in literature. If the receiver is limited by a signal-independent noise (SIN) mechanism (such as thermal noise) that does not beat against the optical signal, and considering a Gaussian distribution for the uncertainty of high and low levels, the power penalty to get the same BER performance and compensate for the signal degradations is estimated as [84]

$$\text{PP}^{\text{SIN}} \approx -10 \log_{10} \left(\frac{\sigma'}{\sigma} \frac{\mu'}{\mu} \right). \tag{5}$$

In contrast, in amplified systems the noise is mainly due to the amplified spontaneous emission (ASE) and that depends on the intensity of the input light to the amplifier (signal dependent noise, SDN). Using the model proposed by Downie [85] that relates the variance of the noise to the high and low levels of the electric field, the power penalty is estimated as

$$\text{PP}^{\text{SDN}} \approx \begin{cases} -10 \log_{10} (\mu'/\mu), & \text{if } \sigma'/\mu' > 1 \\ -10 \log_{10} (\sigma'/\sigma), & \text{if } \sigma'/\mu' \leq 1. \end{cases} \tag{6}$$

This equation implies that the power penalty in this case is related to the worst-case decrease of μ or σ. If the center frequency loses more power than the spectral frequencies, then $\sigma'/\mu' > 1$ and the power penalty is due to the change in μ. If the spectrum loses more power than the center frequency, then $\sigma'/\mu' < 1$, and the penalty is due to the change in σ. In accordance with Eq. (5) and (6), two approaches can be taken to obtain power penalties: 1) Estimate the high and low levels (A' and B') first, and then find μ' and σ' using equations (4a) and (4b). This is the approach we take for characterizing penalties of ring modulators. 2) Directly estimate μ' and σ' based on μ, σ, and the frequency response of the optical device. This is the approach we take for the demultiplexing ring filters.

Also note that in this paper, we mainly work with SIN model and assume no amplification in the link. If amplification is to be considered in the receiver, as it is the case in the experiments against which this work has been compared, Eq. (6) should be employed instead of Eq. (5).

III. Microring Modulators

MRRs are capable of modulating light at very high speeds while operating at low powers. This property combined with the small footprint of these optical modulators turn them into very promising candidates for integrated photonics. The physics behind the operation of such modulators has been well estab-

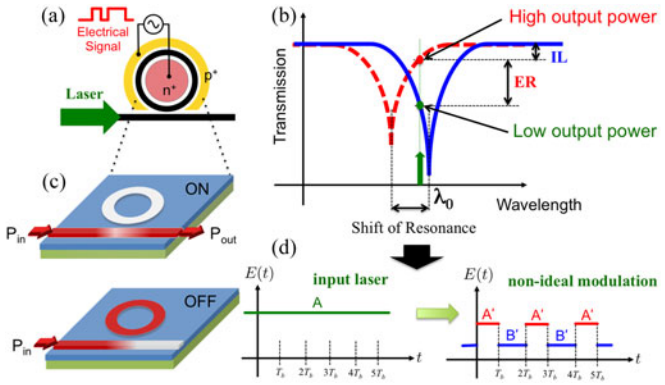

Fig. 3. (a) Schematic view of a microring modulator. The high-speed electrical signal is applied to the p-n-junction embedded inside the silicon ring. (b) Modulation of the input laser by shifting the resonance of the ring to create high and low levels of optical power at the output. (c) Graphical view of how ON and OFF states of the light at the output happen. (d) Time-domain presentation of a non-ideal NRZ OOK modulation.

lished [30]. Just like all other practical modulators, microrings are not capable of providing ideal modulation and thus some impairments and penalties on the optical signal are inevitable. In this section, we provide a general description of the power penalties that are of the most importance.

As depicted in Fig. 3, the electric field envelope of the unmodulated input light has constant amplitude that we denote by A, and constant power $\mathrm{P_{in}} = A^2$. The modulation action occurs by shifting of the resonance of the ring as shown in Fig. 3(b). An ideal NRZ-OOK ring modulator traps the input light depending on whether the data bit is "1" or "0" (shown in Fig. 3(c)). The mean and variance of this ideal modulation (from equations (4a) and (4b)) is $\mu = A/2$, and $\sigma = A/2$, which gives the average power $\mathrm{P_{mod}} = \mu^2 + \sigma^2 = A^2/2 = \mathrm{P_{in}}/2$. We note that $-10\log_{10}(\mathrm{P_{mod}}/\mathrm{P_{in}}) = 3$ dB. As data bits are assumed equiprobable, this means obfuscating half of the power.

A non-ideal modulation differs from the ideal modulation in the way that the high level is A' instead of A ($A' < A$) and the low level is B' instead of zero, so that $\mathrm{P'_{mod}} = \mu'^2 + \sigma'^2 = (A'^2 + B'^2)/2$ as plotted in Fig. 3(d). This causes the power penalty to grow beyond the 3 dB of an ideal modulation. If the transmission of the ring for bit "0" and "1" at the laser wavelength is denoted by T_0 and T_1, then $A' = \sqrt{T_1}$ and $B' = \sqrt{T_0}$. T_0 and T_1 can be estimated by considering a Lorentzian shape for the resonance spectrum of the ring [73]. The ER of modulation is the ratio of power of bit "1" to the power of bit "0", i.e., $r = A'^2/B'^2$. Using equations (4a) and (4b) again, the mean and variance of the non-ideal modulation levels can be written as $\mu' = B'(\sqrt{r}+1)/2$, and $\sigma' = B'(\sqrt{r}-1)/2$. After some further algebraic manipulations[1] the following relations are obtained:

$$\frac{\mu'}{\mu} = \frac{\sqrt{r}+1}{\sqrt{r+1}}\sqrt{\frac{P'_{\mathrm{mod}}}{P_{\mathrm{mod}}}}, \qquad \frac{\sigma'}{\sigma} = \frac{\sqrt{r}-1}{\sqrt{r+1}}\sqrt{\frac{P'_{\mathrm{mod}}}{P_{\mathrm{mod}}}}. \tag{7}$$

[1]In particular, by rewriting levels in terms of average modulation powers $A = \sqrt{2\mathrm{P_{mod}}}$ and $B' = \sqrt{2\mathrm{P'_{mod}}/(r+1)}$.

These can be inserted into Eq. (5) or (6), depending on the noise conditions. Considering a dominant SIN in the system, so Eq. (5), the total modulation power penalty is given by

$$\mathrm{PP^{SIN}_{Mod}} \approx -10\log_{10}\left(\frac{r-1}{r+1}\frac{P'_{\mathrm{mod}}}{P_{\mathrm{mod}}}\right) - 10\log_{10}\left(\frac{P_{\mathrm{mod}}}{P_{\mathrm{in}}}\right) \tag{8}$$

where the second term is the -3 dB corresponding to the ideal modulation. By eliminating $\mathrm{P_{mod}}$ and noting that $\mathrm{P'_{mod}} = (r+1)A'^2/2r$, the power penalty can be rewritten as

$$\mathrm{PP^{SIN}_{Mod}} \approx -10\log_{10}\left(\frac{r-1}{r+1}\right) - 10\log_{10}\left(\frac{A'^2}{P_{\mathrm{in}}}\right) - 10\log_{10}\left(\frac{r+1}{2r}\right). \tag{9}$$

This formulation is helpful as it permits to distinguish three contributing power penalty factors. The first term is the power penalty due to the finite ER of modulation as widely used in the literature [30]. The second term is the modulator insertion loss (IL), defined as the difference between the input power and the power of bit "1." Finally, the third term is the penalty due to the OOK nature of the imperfect modulation. For an ideal modulator (infinite ER and no loss), this last term is 3 dB while the first two terms are reduced to zero.

If a silicon photonic link is dominated by the ASE noise that beats against the optical signal, the power penalty of modulator is estimated from Eq. (6) by noticing that $(\mu'/\mu) > (\sigma'/\sigma)$. The result is

$$\mathrm{PP^{SDN}_{Mod}} \approx -10\log_{10}\left(\frac{\sqrt{r}-1}{\sqrt{r}+1}\right) - 5\log_{10}\left(\frac{P'_{\mathrm{mod}}}{2P_{\mathrm{in}}}\right). \tag{10}$$

The first term in this equation is the power penalty due to the finite ER of modulation (which is different from the one in Eq. (9)) and the second term represents the average power loss due to the combination of OOK and IL of modulator.

Now, we consider several ring modulators mounted on a silicon waveguide, each one modulating a specific wavelength (as in Fig. 1). Cascading all the ring modulators on a single bus waveguide induces two additional power penalties. The first one to be accounted for is the passive cumulative IL of the laser power of each channel as it passes by other rings. If the spacing between wavelengths is small and the number of modulators is large, this could become a significant loss. The second one is the array-induced multiplexing crosstalk [86]. Multiple wavelengths of the comb laser pass by each ring, but only one of them gets modulated. Due to the carrier injection or depletion of the p-n junction of the ring, the spectrum of the ring is switched between two resonance frequencies as shown in the inset of Fig. 4: f_0 (OFF state) and f_1 (ON state), where $f_1 > f_0$ (blue shift). If this shift ($\Delta f = f_1 - f_0$) is too large, then the shifted spectrum may capture some of the power of the neighboring channel that passes by the ring, hence inducing an intermodulation crosstalk. If f_Δ represents the channel spacing and $f_\Delta > 0$, then a neighboring channel at $f_0 + f_\Delta$ would suffer higher crosstalk than a neighboring channel at $f_0 - f_\Delta$. This leads to write the

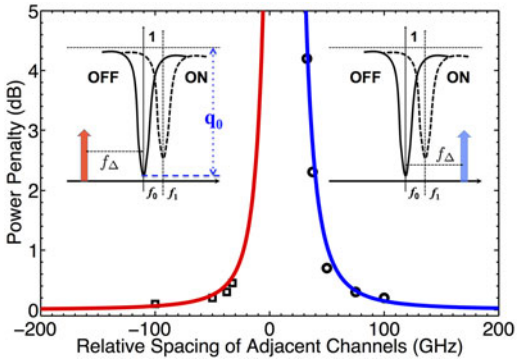

Fig. 4. $\mathrm{PP_{Mod\text{-}Xtalk}}$ (see Eq. (11)) for two cases: (blue) when the adjacent channel is at a higher frequency ($f_\Delta > 0$), (red) when the adjacent channel is at a lower frequency ($f_\Delta < 0$). Due to the unilateral shift of the ring modulator, the first case exhibits higher penalty than the second case. Measurement data [86] are denoted by circles and squares.

worst-case penalty associated with the induced crosstalk as

$$\mathrm{PP_{Mod\text{-}XTalk}} \approx -5\log_{10}\left(\frac{(2\zeta/\mathrm{FWHM})^2 + q_0}{(2\zeta/\mathrm{FWHM})^2 + 1}\right) \tag{11}$$

where $\zeta = f_\Delta - \Delta f$ for $f_\Delta > 0$, and $\zeta = f_\Delta$ for $f_\Delta < 0$. In the above equation, FWHM is the half-power bandwidth of the ring and q_0 is considered as the extinction of the ring resonance in the OFF state ($q_0 = \mathrm{T_{min}/T_{max}}$), where the ring is assumed to be close to critical coupling operation [87]. This power penalty is obtained by assuming a Lorentzian shape for the resonance of the ring.

Using Eq. (11), we reproduce the results of intermodulation crosstalk reported by Padmaraju *et al.* [86] for a microring modulator with $Q \approx 6000$ at the resonance wavelength 1546.7 nm and $q_0 \approx 0.04$. The reproduced results are plotted in Fig. 4 where circles and squares are penalties from experimental data for $f_\Delta > 0$ and $f_\Delta < 0$, respectively.

At this point, we have introduced the main ingredients to estimate the total power penalty induced by a ring-resonator based modulator array. Knowing the parameters Q, coupling coefficients of ring-waveguides, and loss of each ring, its associated Lorentzian transform can be obtained, from which stems A' and B'. These permit to evaluate Eq. (9) or (10), the passive ILs, as well as the intermodulation crosstalk penalty.

IV. Microring Demultiplexers

Consider an NRZ-OOK modulated signal passing through MRR based filter as shown in Fig. 5(a). The filter has two outputs: the drop port and the through port. Considering this filter as a linear time independent system, it can be characterized by two frequency responses $H_{\mathrm{drop}}(f)$ and $H_{\mathrm{through}}(f)$ that relate the output electric field present at each port to the input electric field. Knowing that the input power spectral density is $S_E(f)$, we can calculate the output power spectral density as $S_{\mathrm{out}}(f) = S_E(f)\,|H(f)|^2$ at each port [82]. Unless $H(f)$ is constant for all f, which is not realizable with ring resonators, some degree of spectral distortion will appear. This translates into eye closure in the time domain as shown in Fig. 5(b). At the receiver, the received signal is sampled in each bit interval. We consider this

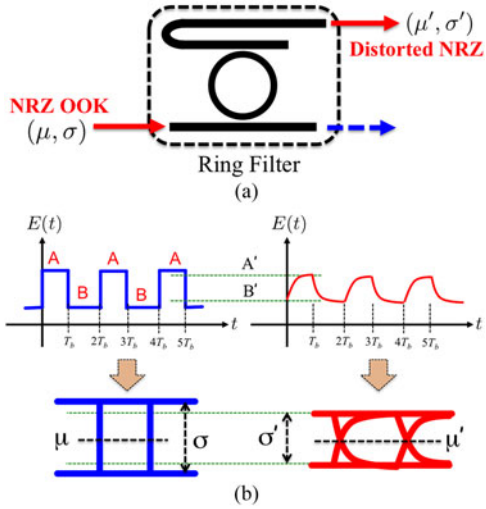

Fig. 5. (a) Schematic representation of a demux ring filter. The input NRZ modulation is characterized by the mean and variance of its high and low levels. The dropped signal is a distorted NRZ modulation that can be characterized by new mean and variance parameters. (b) Comparison between the input NRZ modulation to a filter and its output response. The output is a signal that effectively has new high and low levels A' and B' with different mean and variance than the original signal. This can be seen by inspecting the eye-diagrams of the input and output optical signals.

as a reconstruction of the NRZ-OOK signal with new average high and low levels denoted by A' and B', and new statistical mean μ' and variance σ'^2. Using Eq. (3), the change in the mean and variance by going through the $H(f)$ system can be written as

$$\left(\frac{\mu'}{\mu}\right)^2 \approx |H(f_c)|^2 \tag{12a}$$

$$\left(\frac{\sigma'}{\sigma}\right)^2 \approx \int_{-\infty}^{\infty} |H(f)|^2 \frac{1}{r_b}\mathrm{sinc}^2\left((f - f_c)/r_b\right) df. \tag{12b}$$

The relation between μ and μ' is approximately independent of the shape of the filter since the power associated with the mean of the two levels is centered at a single frequency. On the other hand, the relation between σ and σ' depends on the shape of the filter, indicating spectral distortion to the power spectrum of the signal.

Fig. 6(a) shows demux ring resonators at the receive side of a WDM silicon photonics link, where each one is tuned to drop one of the NRZ-OOK modulated channels. Each ring has an intrinsic loss that corresponds to a decay time-constant denoted by τ_i. The coupling rates and the coupling decay time constants for the ring-waveguide interactions are denoted by (ξ_1, τ_1) and (ξ_2, τ_2) for the through and drop paths as depicted in Fig. 6(b). If the quality factor of the rings is high enough and the coupling of ring-waveguide is weak, one can employ the equations of the temporal coupled mode theory for MRRs [88]. By virtue of the conservation of energy in the ring-waveguide system, the relation between (ξ_1, τ_1) and (ξ_2, τ_2) are then given as $\xi_{1,2} \approx \sqrt{\tau_{1,2}}$ and the drop and through field transfer functions

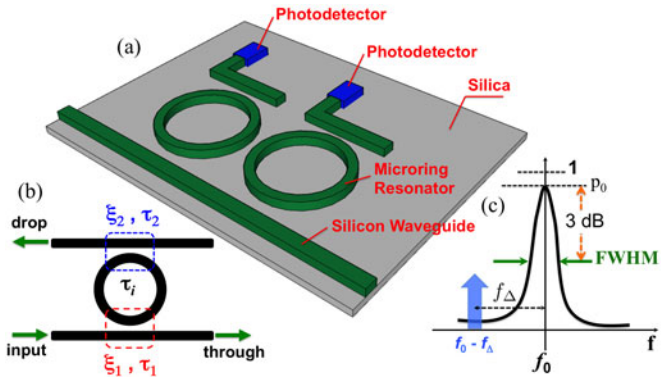

Fig. 6. (a) Graphical view of microring demultiplexers at the receiver. (b) Intrinsic and coupling decay rates of a ring add-drop filter. (c) Transmission spectrum of the drop path of a demux ring with the 3-dB bandwidth denoted as FWHM. f_Δ is the possible detuning between the resonance and the channel.

are

$$H_{\text{drop}}(\Omega) \approx \xi_1 \xi_2 \frac{1}{j\Omega + 1/\tau} \tag{13a}$$

$$H_{\text{through}}(\Omega) \approx \frac{j\Omega + 1/\tau'}{j\Omega + 1/\tau} \tag{13b}$$

where $\Omega = 2\pi(f - f_0)$ is the frequency deviation from the resonance of the ring (f_0), $1/\tau = 1/\tau_i + 1/\tau_2 + 1/\tau_1$, and $1/\tau' = 1/\tau_i + 1/\tau_2 - 1/\tau_1$. The full width at half maximum of the resonance is calculated as FWHM $= 1/(\pi\tau)$, and the quality factor of the resonance is given by $Q = f_0$/FWHM. The power transfer function from the input to the drop port is $|H_{\text{drop}}(\Omega)|^2$, which has a Lorentzian line shape as depicted in Fig. 6(c). The main parameters of this function are the resonance frequency of the ring (f_0), 3-dB bandwidth (FWHM), and the peak drop power ($p_0 = (\xi_1 \xi_2 \tau)^2$).

Once the drop and through shapes of the filter are known, the next step consists of looking at the impact that the drop path has on the spectrum of an NRZ-OOK modulation. This means evaluating the integral of Eq. (12b) for a Lorentzian function. The result is given by

$$\gamma = \frac{1}{1+\beta^2} - \frac{1}{2\pi\nu}\text{Re}\left(\frac{1-\exp(-2\pi\nu(1-j\beta))}{(1-j\beta)^2}\right) \tag{14}$$

in which $\nu = f_0/(2Qr_b)$, $\beta = 2Qf_\Delta/f_0$, and Re(...) indicates the real part of the complex number. Details of calculations are provided in Appendix I. Here, f_Δ denotes any possible detuning between the channel and the resonance of the demux ring as shown in Fig. 6(c).

We note that the first term of Eq. (14) is not a function of bit rate, reflecting only the filtering nature of the device at a distance f_Δ from its resonance. If there is no detuning between the channel and the filter, then $f_\Delta = 0$, $\beta = 0$, and γ is reduced to $\gamma = 1 - (1 - \exp(-2\pi\nu))/(2\pi\nu)$. The second term, on the other hand, depends on the bit rate, highlighting the fact that the bandwidth of the NRZ-OOK signal is a contributor to the spectral distortion imposed by the ring filter. If modulation speed is low enough, the second term is negligible compared to the first term.

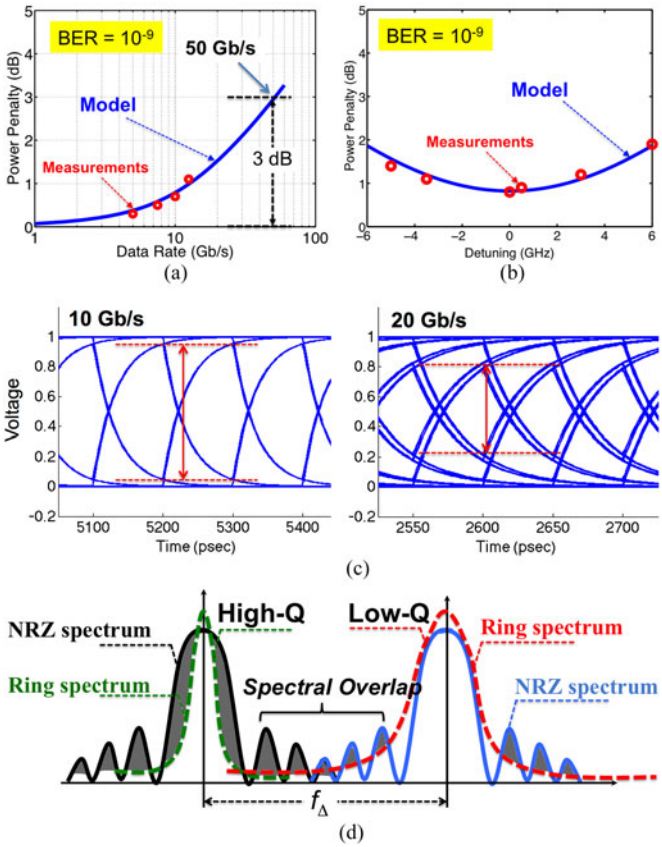

Fig. 7. (a) Comparison of the estimated spectral distortion (solid curve) and measured penalties [71] (circles) for various bit rates. (b) Estimation of the penalty due to small detunings between the resonance of the ring and the channel wavelength. Measurements are taken from [72]. (c) Simulated eye-diagrams of the received signal for 10 and 20 Gb/s data rates. (d) Schematic view of two adjacent channels with a fair amount of spectral overlap. A low-Q ring will result in more crosstalk effect, but less spectral distortion (highlighted areas on the NRZ spectrum). f_Δ denotes the spacing between channels.

We proceed to employ Eq. (14) to evaluate the power penalty of the filtering action. By introducing Eq. (13) into equations (12a) and (12b), we obtain $(\mu'/\mu)^2 \approx p_0/(1+\beta^2)$ and $(\sigma'/\sigma)^2 \approx p_0 \times \gamma$. From there, using Eq. (5), we have

$$\text{PP}^{\text{SIN}}_{\text{Demux}} \approx -10\log_{10}(p_0) - 5\log_{10}\left(\frac{1}{1+\beta^2}\right) - 5\log_{10}(\gamma) \tag{15}$$

for a link with SIN. The first term in PP is simply the drop IL of the resonance spectrum of the ring. The second term reflects the IL at the channel wavelength, and the third term reflects the penalty of spectral distortion due to the filtering. If the link is dominated by an SDN, power penalty is estimated from Eq. (6) as

$$\text{PP}^{\text{SDN}}_{\text{Demux}} \approx -5\log_{10}(p_0) - 5\log_{10}(\gamma). \tag{16}$$

Fig. 7(a) shows the measured power penalties (circles) reported by Biberman *et al.* [71] (at BER $= 10^{-9}$) for a ring of a bandwidth about 10 GHz and four different bit rates: 5 Gb/s (PP $\approx$ 0.3 dB), 7.5 Gb/s (PP $\approx$ 0.5 dB), 10 Gb/s (PP $\approx$ 0.7 dB), and 12.5 Gb/s (PP $\approx$ 1.15 dB). The solid curve on this figure is the estimated power penalty up to 60 Gb/s (PP $\approx$ 3.3 dB) with $f_\Delta = 0$ (exact tuning between the channel and the ring filter).

The model provides a good estimation of the power penalties and predicts a penalty of 3 dB at about 50 Gb/s.

Fig. 7(b) presents the measured penalties (circles) of small detunings (up to 6 GHz) reported by Lee *et al.* [72] (at BER $= 10^{-9}$) for a ring resonator with FWHM $= 9.6$ GHz ($Q \approx 20\,000$) and a bit rate of 10 Gb/s (PP ≈ 0.8 dB at zero detuning). The solid curve represents the estimated BER penalties for a link with SDN mechanism (see equation (16)). The SDN is selected based on the fact that the experiment used optical amplification to compensate for power loss in the system. Here again, we observe good agreement between the measurements and calculations. These two comparisons against measurements let us posit that Eq. (14) can serve as a basis for quantifying the rate-dependent penalties due to sideband truncation of an NRZ-OOK channel.

Fig. 7(c) illustrates the effect of the spectral distortion on the eye-diagram of the received signal for 10 and 20 Gb/s data rates. As it can be observed, the eye-diagram of the 20 Gb/s signal experiences more closure in accordance with higher power penalty.

Besides the spectral distortion of each channel, power penalties also arise in the demultiplexing process in the form of crosstalk. Due to the infinite tail of the Lorentzian resonance and spectral overlap of the channels, capturing and dropping some of the optical power from adjacent channels is unavoidable, as shown in Fig. 7(d). We assume that the worst-case crosstalk happens at the first demux ring in Fig. 1 [66], since all the channels are at their maximum power and none has been dropped yet. The power that is captured by the Lorentzian tail of the ring from the spectra of the adjacent channels has a negative impact on the statistics of the high and low levels at the detector and increases the BER. In order to compensate for this, the crosstalk effect on the BER is turned into a power penalty. The total electric field at the drop port of each demux ring is a superposition of the electric field of the tuned channel and all other crosstalk channels. The worst case of crosstalk happens if all the channels are within the bandwidth of the electronic filter ($|\omega_i - \omega_0| / 2\pi < B_e$) at the receiver (coherent crosstalk). Here we can use Eq. (14) again to characterize the strength of the electric field ($|E(t)|^2$) of the crosstalk channels at the drop port. We also consider a random phase difference between the main channel and each crosstalk channel [89]. In this case, the worst-case of powers of bits "1" and "0" (due to the random phase difference) have the following thresholds:

$$\mathrm{P}_1^{\min} = 1 + \sum_i \gamma_i - 2\sum_i \sqrt{\gamma_i} \tag{17a}$$

$$\mathrm{P}_0^{\max} = \sum_i \gamma_i \tag{17b}$$

where γ_i's are estimated for each crosstalk channel from Eq. (14). The eye-closure penalty then follows from Eq. (5) (SIN) or Eq. (6) (SDN) as

$$\mathrm{PP}^{\mathrm{SIN}}_{\text{Demux-XTalk}} \approx -10\log_{10}\left(\mathrm{P}_1^{\min} - \mathrm{P}_0^{\max}\right) \tag{18a}$$

$$\mathrm{PP}^{\mathrm{SDN}}_{\text{Demux-XTalk}} \approx -10\log_{10}\left(\sqrt{\mathrm{P}_1^{\min}} - \sqrt{\mathrm{P}_0^{\max}}\right). \tag{18b}$$

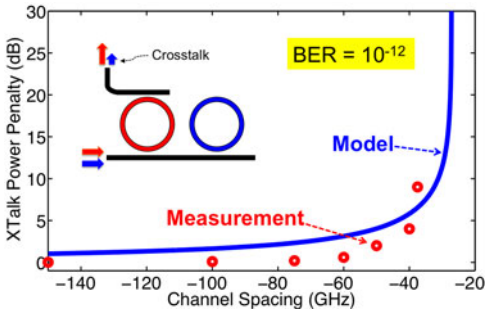

Fig. 8. Comparison of measured crosstalk power penalties (circles) and model (solid line) for two cascaded ring resonators at a bit error rate of 10^{-12}. For channel spacings larger than 1 nm ($\sim$120 GHz), the penalty is negligible. However, penalty sharply increases as the channel spacing is reduced to below 40 GHz. Measurement data are taken from [66].

These equations along with Fig. 7(d) show that penalty of crosstalk between channels depends on the bandwidth of the rings, spacing between channels, and bit rate of each channel. Experimental measurements for the crosstalk penalty between two rings at BER $= 10^{-12}$ have been recently presented in Ref. [66] with a ring bandwidth (FWHM) of 30 GHz and a bit rate of 25 Gb/s (structure shown in the inset of Fig. 8). We compare our estimations to these measurements in Fig. 8 where the solid curve is the estimated power penalty and the circles represent the measured power penalties. A reasonable agreement is observed between measurements and the model. The model tends to overestimate the crosstalk penalty but this is acceptable in a link design context, where one aims at identifying the worst-case scenario.

At this point, we can estimate the worst-case power penalties inflicted by the demux array. Worst-case of crosstalk happens at the first ring, while the worst-case of waveguide loss happens for the last ring. Equations (15) and (16) estimate the impact of truncation while Eq. (18) predicts the effect of crosstalk. Using these equations and the ones presented in the previous section for the modulator side (see Eq. (9)–(11)) , we can proceed to the next steps, which consist of optimizing the ring parameters for minimum power penalty (see Section V) and evaluating the ideal link format ($N_\lambda \times r_b$) for maximum bandwidth (see Section VI).

V. Optimization of Microrings for Minimum Power Penalty

In all of the calculations to follow, we presume an extreme FSR of 50 nm for the rings (which corresponds to approximately 4 μm diameter of the rings). It is also assumed that there is no amplifier in the link, thus the link is dominated by a SIN mechanism.

For the modulators, the parameters subject to optimization are Q-factor of the rings, shift of the resonance due to the plasma dispersion effect, and the spacing between channels. Considering these parameters, trade-offs then should be made between modulator IL, ER penalty, OOK penalty, cumulative arrayed-induced IL, and the multiplexing crosstalk. Fig. 9 shows an example of calculating the total penalty of the ring modulator for a case where channel spacing is 1 nm (hence 50 rings) and

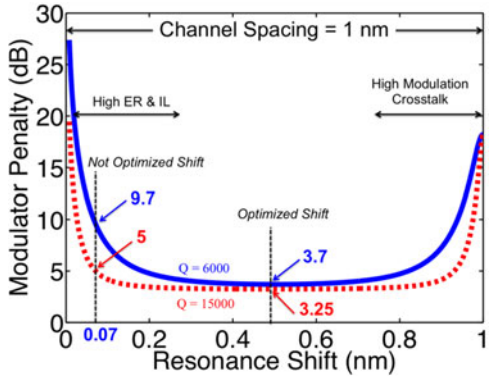

Fig. 9. Estimated modulator penalty for a channel spacing of 1 nm and different resonance shifts. If the shift of the resonance is small, then the IL and ER penalty are high. On the other hand, if the shift is too big, then the crosstalk penalty is very high. The optimum shift is about half of the channel spacing.

the quality factor is either 6000 (low-Q, solid curve) or 15 000 (high-Q, dotted curve). It is assumed that the rings are critically coupled to the waveguide. As this plot indicates, power penalty of a modulator is always higher than 3 dB (which is the penalty of an ideal NRZ-OOK modulator) and the minimum value of the penalty occurs when the shift of the resonance of the ring is approximately half of the channel spacing. Unfortunately, such a big shift of the resonance usually requires high peak-to-peak voltages for the electrical signal that drives the p-n-junction of the ring (according to the formulation presented in [73] and [76]). Consequently, for CMOS-compatible voltages ($V_{pp} \sim 1$–2 V [74], [90]), the resonance shift is away from its optimum value and this leads to higher penalties on the modulators. For example in Fig. 9, a shift of about 0.5 nm leads to a penalty of 3.7 dB for $Q = 6000$ and a shift of 0.07 nm ($\sim$ 8.5 GHz) leads to about 9.7 dB penalty. It is important to note that here we make the assumption that the ring modulators are driven with pre-emphasized NRZ signals to effectively compensate for the limited bandwidth of the modulator [40]. Hence, we always consider that the static ER can be achieved under dynamic drive. With this assumption, higher Q factor for the ring modulators is more desirable as it reduces the penalty of the modulator for a fixed amount of resonance shift. This fact can be seen on Fig. 9.

For the ring demultiplexers, the parameters subject to optimization are the Q-factor of the rings, bit rate of channels, and channel spacing. Trade-offs are then established among drop IL, spectral distortion, and crosstalk penalties. As an example, Fig. 10(a) shows the optimized overall penalty of demux rings for 50 channels with 1 nm spacing between them, various bit rates, and various Q-factors. This penalty is the sum of the spectral distortion (see Eq. (15)), the cross-talk penalty (see Eq. (18a)) and ring drop IL. The latter is function of the intrinsic loss of the ring α_{loss} and Q-factor (as developed in Appendix II). Note that the intrinsic loss is not subject to optimization: the minimal value that fabrication can provide should simply be employed to limit IL. In contrast, the Q-factor can clearly be optimized if the objective is to minimize the overall power penalty. Looking at Fig 10(a), one notes that if the Q of the ring is small, crosstalk has a big impact on the penalty. On the other hand, if the Q is too high, then the spectral distortion penalty and

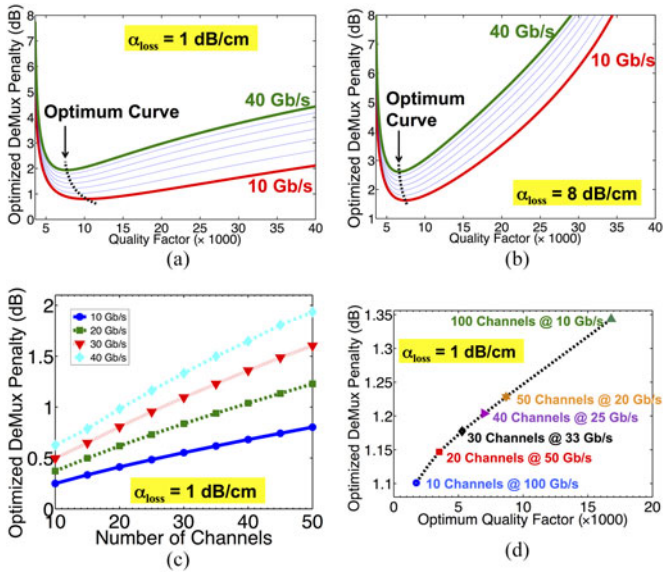

Fig. 10. Optimizing the penalty of demux ring filters by including the IL as a function of Q-factor of the ring. (a) Loss factor of the ring is 1 dB/cm and 50 channels. (b) Loss factor of the ring is 8 dB/cm and 50 channels. (c) Power penalty for different number of channels and bit rates (loss = 1 dB/cm) when using demux rings with optimized Q. (d) Optimum penalty and its corresponding Q-factor for an aggregate rate of 1 Tb/s and different channel rates (loss = 1 dB/cm).

IL have higher impacts. Therefore, there is a minimum point for the power penalty at an optimum Q-factor. The dependence of the optimum penalty and optimum Q on the bit rate is emphasized on Fig. 10(a) with the dotted black curve showing how the optimum point behaves as the bit rate increases. This indicates that higher bit rates lead to wider filters in order to compensate for higher spectral distortion. In Fig. 10(b), same optimization is done for the demux rings but with 8 dB/cm ring loss [66]. It is clear that in this case, high-Q rings will lead to a high IL. In Fig. 10(c) we plot the penalty of different bit rates and different number of channels for optimally set Q-factors. It is seen that penalty tends to increase as the spacing between channels decreases. Finally, we perform the optimization on microring demux filter with the assumption of having a fixed amount of total aggregate rate (1 Tb/s is assumed). In this case, increasing the number of channels, e.g., from 10 to 100, is accompanied by a decrease in the modulation speed. The results are shown in Fig. 10(d) where six cases are clearly marked on the plot. With optimum design of the rings, the penalties result in a narrow range 1.1–1.35 dB. Meanwhile, the corresponding quality factors can vary over a wide range from 1800 to 17 000.

VI. Scalability Analysis of a Microring-Based Silicon Photonic Link

The scalability of a silicon photonic link in terms of the maximum total aggregate rate depends on the available optical power budget. Based on the characterization of power penalties for ring modulators at the transmitter and ring demultiplexers at the receiver, it is possible to maximize the achievable aggregation. For each particular bit-rate, the analysis is carried out by finding the maximum value of N_λ such that Eq. (1) holds. This

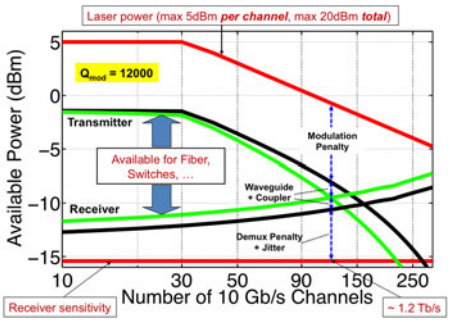

Fig. 11. Calculation of the available optical power at the output of the transmitter and minimum required power at the input of the receiver. Both calculations reflect the worst-case. The difference is the available power budget for losses and penalties associated with fibers, or switches that are placed between transmitter and receiver. The capacity of the link is estimated to be 1.2 Tb/s. Quality factor of ring modulators is taken to be 12 000 and intrinsic loss factor α_{loss} to be 1 dB/cm.

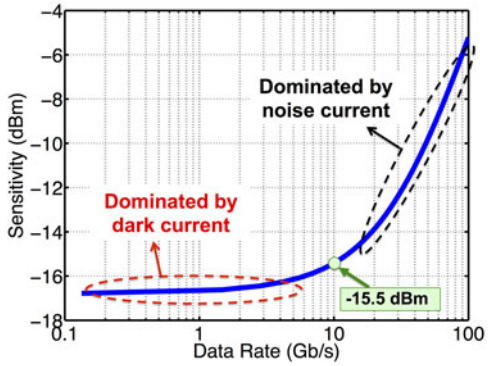

Fig. 12. Estimated sensitivity of the receiver as a function of the modulation data rate. At low data rates, dark current dominates over the noise current and thus the sensitivity is almost constant, whereas at high data rates the noise current dominates over the dark current and sensitivity is reduced.

is done by incorporating power penalties from Eq. (9) or (10), (11), (15) or (16), and (18) into the PP_{tot} term in Eq. (1). Some of the power penalties of the link do not generally depend on the bit-rate of channels or on the number of channels/channel spacing. Examples include the waveguide propagation loss ($\sim$ 1 dB/cm) and chip-to-fiber/fiber-to-chip coupling IL ($\sim$ 1 dB) [74]. The penalties of the modulators are also approximately independent of bit-rate, but depend on the number of channels due to array-induced IL and inter-modulation crosstalk. This can be taken as an encouragement to use higher bit-rates at the modulators. However, higher bit-rates limit the sensitivity of the receiver circuitry which, as we will see, eventually puts a cap on the maximum achievable bandwidth. Overall, this engenders an interesting design space to explore.

We initiate our explorations by calculating the available power at the output of the transmitter chip and the minimum required power at the input of the receiver as a function of number of channels for 10 Gb/s NRZ-OOK modulation, as shown in Fig. 11. It is assumed that laser can provide a maximum power of 5 dBm for each wavelength (after coupling into the waveguide), but the total amount of the optical power that is injected into the silicon waveguide is kept below 20 dBm to avoid the nonlinearities of the silicon waveguide. The sensitivity of the receiver for each channel is set to a value of -15.5 dBm (given by a rate-dependent model, to be described later). These assumptions set the limit of the maximum power budget to 20.5 dB for each 10 Gb/s channel. From the transmitter side, we add up the modulator penalties (loss, ER, crosstalk) and the waveguide loss, assuming 1 dB/cm loss for the silicon waveguide. Since the number of required modulators and demultiplexers is equal to the number of channels, the length of the waveguides linearly scales up with the number of channels. Then, we add up the worst-case penalty associated with the demultiplexers (including worst-case crosstalk and worst-case waveguide loss). We also account for a 2 dB extra margin to compensate jitter in clocking. In contrast, we do not account for power penalties related to chromatic dispersion. We assume this last to be negligible for short distance links with modulation rates $<$ 100 Gb/s. Fig. 11 shows that at about 120 channels, the power budget completely closes and thus the scalability of this link for 10 Gb/s channels is limited to about 1.2 Tb/s. For lower number of channels, there is some budget remaining. It can be exploited to introduce additional elements in the link (more couplers, switches, etc.). Alternatively, launching powers per channel can be reduced to limit the power consumption of the laser.

Next, the dependence of the scalability of the link on the modulation speed is investigated. In this case, we still assume the same condition on laser power (5 dBm per channel, maximum 20 dBm total), but a bit-rate dependent model for the sensitivity of Germanium-based detector is employed. The model for the sensitivity is based on the simple definition of the BER for OOK modulation with Gaussian noise at the receiver. Therefore, sensitivity is defined by the following equation:

$$\text{P}_{\text{sensitivity}} \approx 10\log_{10}\left(Q_{\text{BER}}\frac{I_{\text{dark}}+I_{\text{noise}}^{\text{RMS}}}{R}\frac{10^{\text{ER}/10}+1}{10^{\text{ER}/10}-1}\right) \quad (19)$$

where Q_{BER} is the argument of the complementary error function ($Q_{\text{BER}} = 7$ for $\text{BER} = 10^{-12}$), R is a responsivity [A/W] of the photodiode (assumed $\sim$0.7 A/W), ER is the extinction ratio of input signal [dB] (assumed $\sim$10 dB as a reference), I_{dark} is the dark current [mA] (assumed $\sim$1 μA) and I_{noise} is the total RMS input-referred noise current [mA] of the receiver [19], [91]–[95]. For simplicity, we also assume that the receiver has enough bandwidth to accommodate the designated bit rate (BW $\approx$ 0.75 DataRate). The noise current is estimated from an input-referred RC equivalent circuit for the receiver (photodiode + TIA) whose 3 dB bandwidth is set to the bandwidth of the receiver [19]. Fig. 12 shows a plot of the obtained sensitivity for $\text{BER} = 10^{-12}$. The sensitivity is dominated by dark current at low data rates, whereas at high data rates is dominated by the noise current. A sensitivity of -15.5 dBm is then obtained for 10 Gb/s NRZ OOK modulation.

We identify the highest number of channels supported for each modulation rate up to 120 Gb/s (see Fig. 13). By evaluating the link format ($N_\lambda \times r_b$ product), it is found that a chip-to-chip silicon photonic link, under the considered assumptions, can support a peak aggregated bandwidth of $\sim$2.1 Tb/s, composed of 47 channels at 45 Gb/s. This corresponds to a channel spacing of 1.06 nm (i.e., $\sim$125 GHz) and a modulator shift of 0.53 nm. The

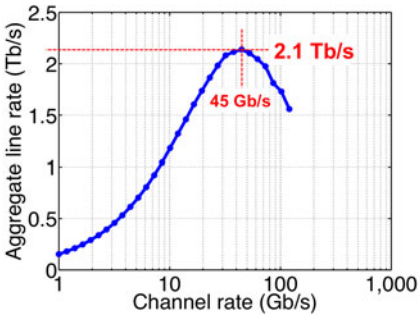

Fig. 13. Plot of estimated maximum capacity of the link based on the power penalties of the link and the modulation rate of each channel. It is seen that the link can support up to 2.1 Tb/s at a modulation rate of 45 Gb/s. If 10 Gb/s modulation is used, the total capacity is 1.2 Tb/s as shown in Fig. 11.

breakdown of the power penalties in this case includes 5.56 dB for the modulator array (Eq. (9) + Eq. (11) + cumulative IL of the array), 1.6 dB for waveguide loss and coupling at the transmitter side, negligible fiber loss and dispersion effects (considering a short-reach application), 1.2 dB for waveguide loss and coupling at the receiver, 3.5 dB for the optimized demultiplexing array, and 2 dB for jitter penalty. The overall power penalty at 45 Gb/s for 47 channels then sums up to 13.8 dB which is equal to the total power budget per wavelength (3.4 dBm laser power for each channel, and -10.4 dBm receiver sensitivity).

Overall, this result is to be considered with care, as the generation and detection of 45 Gb/s electric signal might be problematic and energy consuming. Nevertheless, it is a good indicator of the general capabilities of silicon photonics ring resonators from an optical point-of-view.

VII. Conclusion

The paper provided a comprehensive design and modeling platform for a detailed link level analysis of a silicon photonic WDM link realized with microrings. It characterized power penalties of microring modulators and presented a closed-form approximation for the spectral distortion of a microring filter for NRZ-OOK modulated signals. The theoretical estimations for the penalties of spectral distortion and their dependence on the modulation speed (bit-rate) were compared and verified against experimental measurements. Crosstalk effects at the transmitter and the receiver were estimated and we showed that the models for crosstalk agree with the experimental measurements. Based on the presented models, we explored optimal device parameters to minimize the overall power penalties of the link. Our design space exploration indicates that with the current state of the art photonic components and optimal microring parameters, the best possible modulation rate for each channel, and the total aggregate link rate are approximately 45 Gb/s and 2.1 Tb/s, respectively.

Appendix I

In accordance with Eq. (12b) and Eq. (13), the variance of the NRZ-OOK modulation changes by getting dropped by the ring as $(\sigma'/\sigma)^2 = p_0 \times \gamma$ where

$$\gamma = \int_{-\infty}^{\infty} \frac{\mathrm{sinc}^2(F)}{1 + ((F - F_\Delta)/\nu)^2} dF \tag{A1}$$

$\nu = \mathrm{FWHM}/(2r_b)$, and $F_\Delta = f_\Delta / r_b$. In order to calculate this integral, one has to employ the residue theorem. Rewriting the integral in the form of

$$\gamma = \frac{\nu^2}{2\pi^2} \mathrm{Re} \int_{-\infty}^{\infty} \frac{1 - \exp(j2\pi F)}{F^2((F - F_\Delta)^2 + \nu^2)} dF \tag{A2}$$

and choosing the appropriate contour in the upper half plane shown in Fig. 14 indicates that there is only one pole at $Z_0 = F_\Delta + j\nu$ inside this contour. The closed-loop integral is then calculated as

$$\oint \frac{1 - \exp(j2\pi Z)}{Z^2((Z - F_\Delta)^2 + \nu^2)} dZ = \frac{\pi}{\nu Z_0^2}(1 - \exp(j2\pi Z_0)). \tag{A3}$$

Obviously, due to the higher-order denominator, the integral over $C(\infty)$ is zero. The integral over $C(\varepsilon)$ where $\varepsilon \to 0$ on the other hand is not zero and must be calculated. Substituting $Z = \varepsilon \exp(j\theta)$ into the integrand of Eq. (A3), will then yield the following result

$$\int_{C(\epsilon)} \frac{1 - \exp(j2\pi Z)}{Z^2((Z - F_\Delta)^2 + \nu^2)} dZ = \frac{-2\pi^2}{|Z_0|^2}. \tag{A4}$$

Combining the above equations finally leads to

$$\gamma = \frac{\nu^2}{|Z_0|^2} + \frac{\nu}{2\pi} \mathrm{Re}\left(\frac{1 - \exp(j2\pi Z_0)}{Z_0^2}\right) \tag{A5}$$

which can also be cast as Eq. (14).

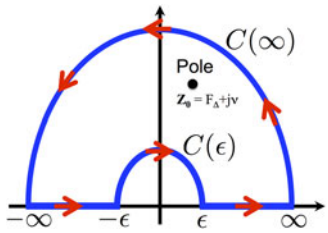

Fig. 14. Selected contour in the upper half-plane for evaluating the integral of the spectral distortion penalty. There is a pole at the origin and a pole at $Z_0 = F_\Delta + j\nu$.

Appendix II

Considering the Lorentzian function presented in Eq. (13), the goal is to minimize the IL (make it as close as possible to 0 dB) of the drop path of the demux ring. For convenience, we introduce the normalized rate parameters as $x = (1/\tau_1)/(1/\tau_i)$ and $y = (1/\tau_2)/(1/\tau_i)$. For a demux ring, the drop IL is $|H_{\mathrm{drop}}(0)|^2 = 4xy/(1 + x + y)^2$. This expression is completely symmetric for both x and y. Considering a given value for y, equating the derivative of the $|H_{\mathrm{drop}}(0)|^2$ with respect to x to zero yields $x_{\mathrm{opt}} = 1 + y$ which is exactly the critical coupling condition (input coupling rate is equal to the intrinsic loss rate plus the output coupling rate) for a ring resonator. Substituting x_{opt} then gives

$|H_{\text{drop}}(0)|^2 = y/(1+y)$ and thus y must be chosen large enough to get as close to 0 dB as possible. A large y can correspond to a big τ_i which in turn corresponds to a low loss ring. Substituting for $\tau_i \approx 2n_g/(c\,\alpha_{\text{loss}})$ where n_g is the group index, α_{loss} is the loss factor (1/m) of the ring (including waveguide loss and bending loss) and $c = 3 \times 10^8$ m/s is the speed of light, the minimum IL of drop path (in dB) is calculated as

$$\text{IL}_{\text{Demux}} = -10\log_{10}\left(1 - \frac{2Q}{Q_i}\right) \tag{A6}$$

where the intrinsic quality factor is $Q_i = 2\pi n_g/(\alpha_{\text{loss}}\lambda_0)$, and λ_0 is the resonance wavelength of the ring. As indicated in Fig. 10, for a ring that has a high loss factor the optimization is very critical, otherwise the power penalty can rise very quickly. This figure also suggests that the optimum design for a demux filter is to have it as low-loss as possible at the critical coupling point. The coupling coefficients of the electric field between the waveguide and the ring at the input and drop ports of the demux ring are then estimated as

$$\kappa_1 \approx \sqrt{(2\pi R\,\alpha_{\text{loss}})x}, \qquad \kappa_2 \approx \sqrt{(2\pi R\,\alpha_{\text{loss}})y} \tag{A7}$$

where $2\pi R$ is the circumference of the ring, α_{loss} is the loss factor of the ring expressed in 1/m, and $x = 1 + y$ at the critical coupling point. These coupling coefficients can be used to estimate the gap distances between the ring and the waveguides.

ACKNOWLEDGMENT

Sandia National Laboratories is a multi-program laboratory managed and operated by Sandia Corporation, a wholly owned subsidiary of Lockheed Martin Corporation, for the U.S. Department of Energy's National Nuclear Security Administration under Contract DE-AC04-94AL85000. The authors would like to thank Dr. N. Ophir and T. Shiraishi for enlightening discussions.

REFERENCES

[1] J. Ahn, M. Fiorentino, R. G. Beausoleil, N. Binkert, A. Davis, D. Fattal, N. P. Jouppi, M. McLaren, C. M. Santori, R. S. Schreiber *et al.*, "Devices and architectures for photonic chip-scale integration," *Appl. Phys. A*, vol. 95, no. 4, pp. 989–997, 2009.

[2] G. T. Reed, W. R. Headley, and C. J. Png, "Silicon photonics: The early years," *Proc. SPIE, Integr. Optoelectronic Devices*, vol. 5730, pp. 1–18, 2005.

[3] R. Soref, "The past, present, and future of silicon photonics," *IEEE J. Select. Topics Quantum Electron.*, vol. 12, no. 6, pp. 1678–1687, Nov./Dec. 2006.

[4] L. Tsybeskov, D. J. Lockwood, and M. Ichikawa, "Silicon photonics: CMOS going optical [scanning the issue]," *Proc. IEEE*, vol. 97, no. 7, pp. 1161–1165, Jul. 2009.

[5] Y. Arakawa, T. Nakamura, Y. Urino, and T. Fujita, "Silicon photonics for next generation system integration platform," *IEEE Commun. Mag.*, vol. 51, no. 3, pp. 72–77, Mar. 2013.

[6] A. K. K. Ziabari, J. L. Abellán, R. Ubal, C. Chen, A. Joshi, and D. Kaeli, "Leveraging silicon-photonic NoC for designing scalable GPUs," in *Proc. 29th ACM Int. Conf. Supercomput.*, 2015, pp. 273–282.

[7] D. Dang, B. Patra, R. Mahapatra, and M. Fiers, "Mode-division-multiplexed photonic router for high performance network-on-chip," in *Proc. IEEE 28th Int. Conf. VLSI Des.*, 2015, pp. 111–116.

[8] A. Shacham, K. Bergman, and L. P. Carloni, "On the design of a photonic network-on-chip," in *Proc. IEEE Ist Int. Symp. Networks-on-Chip*, 2007, pp. 53–64.

[9] A. Shacham, K. Bergman, and L. P. Carloni, "Photonic networks-on-chip for future generations of chip multiprocessors," *IEEE Trans. Comput.*, vol. 57, no. 9, pp. 1246–1260, Sep. 2008.

[10] T. Hu, C. Qiu, P. Yu, L. Yang, W. Wang, X. Jiang, M. Yang, L. Zhang, and J. Yang, "Silicon photonic network-on-chip and enabling components," *Sci. China Technol. Sci.*, vol. 56, no. 3, pp. 543–553, 2013.

[11] D. Nikolova, S. Rumley, D. Calhoun, Q. Li, R. Hendry, P. Samadi, and K. Bergman, "Scaling silicon photonic switch fabrics for data center interconnection networks," *Opt. Exp.*, vol. 23, no. 2, pp. 1159–1175, 2015.

[12] A. V. Krishnamoorthy, R. Ho, X. Zheng, H. Schwetman, J. Lexau, P. Koka, G. Li, I. Shubin, and J. E. Cunningham, "Computer systems based on silicon photonic interconnects," *Proc. IEEE*, vol. 97, no. 7, pp. 1337–1361, Jul. 2009.

[13] Y. A. Vlasov, "Silicon CMOS-integrated nano-photonics for computer and data communications beyond 100g," *IEEE Commun. Mag.*, vol. 50, no. 2, pp. s67–s72, Feb. 2012.

[14] S. Rumley, D. Nikolova, R. Hendry, Q. Li, D. Calhoun, and K. Bergman, "Silicon photonics for exascale systems," *J. Lightw. Technol.*, vol. 33, no. 3, pp. 547–562, Feb. 2015.

[15] P. W. Coteus, J. U. Knickerbocker, C. H. Lam, and Y. A. Vlasov, "Technologies for exascale systems," *IBM J. Res. Develop.*, vol. 55, no. 5, pp. 14:1–14:12, 2011.

[16] D. A. Miller, "Device requirements for optical interconnects to silicon chips," *Proc. IEEE*, vol. 97, no. 7, pp. 1166–1185, Jul. 2009.

[17] M. Haurylau, G. Chen, H. Chen, J. Zhang, N. A. Nelson, D. H. Albonesi, E. G. Friedman, and P. M. Fauchet, "On-chip optical interconnect roadmap: Challenges and critical directions," *IEEE J. Select. Topics Quantum Electron.*, vol. 12, no. 6, pp. 1699–1705, Nov./Dec. 2006.

[18] F. Y. Liu, D. Patil, J. Lexau, P. Amberg, M. Dayringer, J. Gainsley, H. F. Moghadam, X. Zheng, J. E. Cunningham, A. V. Krishnamoorthy *et al.*, "10-Gbps, 5.3-mw optical transmitter and receiver circuits in 40-nm CMOS," *IEEE J. Solid-State Circuits*, vol. 47, no. 9, pp. 2049–2067, Sep. 2012.

[19] J. F. Buckwalter, X. Zheng, G. Li, K. Raj, and A. V. Krishnamoorthy, "A monolithic 25-Gb/s transceiver with photonic ring modulators and Ge detectors in a 130-nm CMOS SOI process," *IEEE J. Solid-State Circuits*, vol. 47, no. 6, pp. 1309–1322, Jun. 2012.

[20] D. M. Gill, J. E. Proesel, C. Xiong, J. S. Orcutt, J. C. Rosenberg, M. H. Khater, T. Barwicz, S. Assefa, S. M. Shank, C. Reinholm *et al.*, "Demonstration of a high extinction ratio monolithic CMOS integrated nanophotonic transmitter and 16 Gb/s optical link," *IEEE J. Select. Topics Quantum Electron.*, vol. 21, no. 4, pp. 1–11, Jul./Aug. 2015.

[21] I. Shubin, X. Zheng, H. Thacker, S. S. Djordjevic, S. Lin, P. Amberg, J. Yao, J. Lexau, E. Chang, F. Liu *et al.*, "Microring-based multi-chip WDM photonic module," *Opt. Exp.*, vol. 23, no. 10, pp. 13 172–13 184, 2015.

[22] R. Ding, Y. Liu, Q. Li, Z. Xuan, Y. Ma, Y. Yang, A.-J. Lim, G.-Q. Lo, K. Bergman, T. Baehr-Jones et al.,"A compact low-power 320-Gb/s WDM transmitter based on silicon microrings," *IEEE Photon. J.*, vol. 6, no. 3, pp. 1–8, Jun. 2014.

[23] P. Dong, W. Qian, H. Liang, R. Shafiiha, N.-N. Feng, D. Feng, X. Zheng, A. V. Krishnamoorthy, and M. Asghari, "Low power and compact reconfigurable multiplexing devices based on silicon microring resonators," *Opt. Exp.*, vol. 18, no. 10, pp. 9852–9858, 2010.

[24] P. Dong, S. Liao, D. Feng, H. Liang, D. Zheng, R. Shafiiha, C.-C. Kung, W. Qian, G. Li, X. Zheng *et al.*, "Low Vpp, ultralow-energy, compact, high-speed silicon electro-optic modulator," *Opt. Exp.*, vol. 17, no. 25, pp. 22 484–22 490, 2009.

[25] W. Bogaerts, R. Baets, P. Dumon, V. Wiaux, S. Beckx, D. Taillaert, B. Luyssaert, J. Van Campenhout, P. Bienstman, and D. Van Thourhout, "Nanophotonic waveguides in silicon-on-insulator fabricated with CMOS technology," *J. Lightw. Technol.*, vol. 23, no. 1, pp. 401–412, Jan. 2005.

[26] W. Bogaerts, P. De Heyn, T. Van Vaerenbergh, K. De Vos, S. Kumar Selvaraja, T. Claes, P. Dumon, P. Bienstman, D. Van Thourhout, and R. Baets, "Silicon microring resonators," *Laser Photon. Rev.*, vol. 6, no. 1, pp. 47–73, 2012.

[27] B. G. Lee, A. Biberman, J. Chan, and K. Bergman, "High-performance modulators and switches for silicon photonic networks-on-chip," *IEEE J. Select. Topics Quantum Electron.*, vol. 16, no. 1, pp. 6–22, Jan./Feb. 2010.

[28] Q. Xu, B. Schmidt, S. Pradhan, and M. Lipson, "Micrometre-scale silicon electro-optic modulator," *Nature*, vol. 435, no. 7040, pp. 325–327, 2005.

[29] S. Lin, E. Schonbrun, and K. Crozier, "Optical manipulation with planar silicon microring resonators," *Nano Lett.*, vol. 10, no. 7, pp. 2408–2411, 2010.

[30] G. Li, A. V. Krishnamoorthy, I. Shubin, J. Yao, Y. Luo, H. Thacker, X. Zheng, K. Raj, and J. E. Cunningham, "Ring resonator modulators in silicon for interchip photonic links," *IEEE J. Select. Topics Quantum Electron.*, vol. 19, no. 6, pp. 95–113, Nov./Dec. 2013.

[31] L. Zhang, Y. Li, M. Song, J.-Y. Yang, R. G. Beausoleil, and A. E. Willner, "Silicon microring-based signal modulation for chip-scale optical interconnection," *Appl. Phys. A*, vol. 95, no. 4, pp. 1089–1100, 2009.

[32] G. T. Reed, G. Mashanovich, F. Gardes, and D. Thomson, "Silicon optical modulators," *Nature Photon.*, vol. 4, no. 8, pp. 518–526, 2010.

[33] P. Dong, R. Shafiiha, S. Liao, H. Liang, N.-N. Feng, D. Feng, G. Li, X. Zheng, A. V. Krishnamoorthy, and M. Asghari, "Wavelength-tunable silicon microring modulator," *Opt. Exp.*, vol. 18, no. 11, pp. 10 941–10 946, 2010.

[34] C. Manolatou and M. Lipson, "All-optical silicon modulators based on carrier injection by two-photon absorption," *J. Lightw. Technol.*, vol. 24, no. 3, pp. 1433–1439, Mar. 2006.

[35] R. A. Soref and B. R. Bennett, "Electrooptical effects in silicon," *IEEE J. Quantum Electron.*, vol. 23, no. 1, pp. 123–129, Jan. 1987.

[36] S. Stepanov and S. Ruschin, "Modulation of light by light in silicon-on-insulator waveguides," *Appl. Phys. Lett.*, vol. 83, no. 25, pp. 5151–5153, 2003.

[37] Q. Li, Y. Liu, K. Padmaraju, R. Ding, D. F. Logan, J. J. Ackert, A. P. Knights, T. Baehr-Jones, M. Hochberg, and K. Bergman, "10-Gb/s BPSK link using silicon microring resonators for modulation and demodulation," presented at the Optical Fiber Communication Conf., San Francisco, CA, USA, 2014, Paper Tu2E-5.

[38] Y. Liu, R. Ding, Q. Li, Y. Ma, Y. Yang, A. E.-J. Lim, G.-Q. Lo, K. Bergman, T. Baehr-Jones, and M. Hochberg, "40-Gb/s silicon modulators for mid-reach applications at 1550 nm," in *Proc. IEEE Opt. Interconnects Conf.*, 2014, pp. 19–20.

[39] T. Baba, S. Akiyama, M. Imai, N. Hirayama, H. Takahashi, Y. Noguchi, T. Horikawa, and T. Usuki, "50-Gb/s ring-resonator-based silicon modulator," *Opt. Exp.*, vol. 21, no. 10, pp. 11 869–11 876, 2013.

[40] Q. Xu, S. Manipatruni, B. Schmidt, J. Shakya, and M. Lipson, "12.5 Gbit/s carrier-injection-based silicon micro-ring silicon modulators," *Opt. Exp.*, vol. 15, no. 2, pp. 430–436, 2007.

[41] T. Gu, Y.-K. Chen, C. W. Wong, and P. Dong, "Cascaded uncoupled dual-ring modulator," *Opt. Lett.*, vol. 39, no. 16, pp. 4974–4977, 2014.

[42] X. Zheng, I. Shubin, G. Li, T. Pinguet, A. Mekis, J. Yao, H. Thacker, Y. Luo, J. Costa, K. Raj *et al.*, "A tunable 1×4 silicon CMOS photonic wavelength multiplexer/demultiplexer for dense optical interconnects," *Opt. Exp.*, vol. 18, no. 5, pp. 5151–5160, 2010.

[43] J. Wang, "Recent progress in on-chip multiplexing/demultiplexing silicon photonic devices and technologies," in *PIERS Proc.*, 2014, pp. 368–373.

[44] J. E. Cunningham, I. Shubin, X. Zheng, T. Pinguet, A. Mekis, Y. Luo, H. Thacker, G. Li, J. Yao, K. Raj *et al.*, "Highly-efficient thermally-tuned resonant optical filters," *Opt. Exp.*, vol. 18, no. 18, pp. 19 055–19 063, 2010.

[45] M. S. Dahlem, C. W. Holzwarth, A. Khilo, F. X. Kärtner, H. I. Smith, and E. P. Ippen, "Reconfigurable multi-channel second-order silicon microring-resonator filterbanks for on-chip wdm systems," *Opt. Exp.*, vol. 19, no. 1, pp. 306–316, 2011.

[46] S. Xiao, M. H. Khan, H. Shen, and M. Qi, "Multiple-channel silicon micro-resonator based filters for WDM applications," *Opt. Exp.*, vol. 15, no. 12, pp. 7489–7498, 2007.

[47] M. A. Popovic, T. Barwicz, M. R. Watts, P. T. Rakich, L. Socci, E. P. Ippen, F. X. Kärtner, and H. I. Smith, "Multistage high-order microring-resonator add-drop filters," *Opt. Lett.*, vol. 31, no. 17, pp. 2571–2573, 2006.

[48] C. Nitta, M. Farrens, and V. Akella, "Addressing system-level trimming issues in on-chip nanophotonic networks," in *Proc. IEEE 17th Int. Symp. High Performance Comput. Archit.*, 2011, pp. 122–131.

[49] Q. Li, N. Ophir, L. Xu, K. Padmaraju, L. Chen, M. Lipson, and K. Bergman, "Experimental characterization of the optical-power upper bound in a silicon microring modulator," in *Proc. IEEE Opt. Interconnects Conf.*, 2012, pp. 38–39.

[50] E. Timurdogan, A. Biberman, D. C. Trotter, C. Sun, M. Moresco, V. Stojanovic, and M. R. Watts, "Automated wavelength recovery for microring resonators," presented at the Conf. Laser Electro-Optic, San Jose, CA, USA, 2012, Paper CM2M-1.

[51] W. A. Zortman, A. L. Lentine, D. C. Trotter, and M. R. Watts, "Bit-error-rate monitoring for active wavelength control of resonant modulators," *IEEE Micro*, vol. 33, no. 1, pp. 42–52, Jan. 2013.

[52] J. A. Cox, A. L. Lentine, D. C. Trotter, and A. L. Starbuck, "Control of integrated micro-resonator wavelength via balanced homodyne locking," *Opt. Exp.*, vol. 22, no. 9, pp. 11 279–11 289, 2014.

[53] K. Padmaraju, J. Chan, L. Chen, M. Lipson, and K. Bergman, "Dynamic stabilization of a microring modulator under thermal perturbation," presented at the Optical Fiber Communication Conf., Los Angeles, CA, USA, 2012, Paper OW4F–2.

[54] K. Padmaraju, J. Chan, L. Chen, M. Lipson, and K. Bergman, "Thermal stabilization of a microring modulator using feedback control," *Opt. Exp.*, vol. 20, no. 27, pp. 27 999–28 008, 2012.

[55] K. Padmaraju, D. F. Logan, J. J. Ackert, A. P. Knights, and K. Bergman, "Wavelength locking of microring resonators and modulators using a dithering signal," in *Proc. 39th Eur. Conf. Exhib. Opt. Commun.*, 2013, pp. 1–3.

[56] P. Dong, S. F. Preble, and M. Lipson, "All optical ultrafast broadband silicon switch," presented at the Conf. Lasers Electro-Optics, Baltimore, MD, USA, 2007, Paper CTuDD2.

[57] B. G. Lee, A. Biberman, P. Dong, M. Lipson, and K. Bergman, "All-optical comb switch for multiwavelength message routing in silicon photonic networks," *IEEE Photon. Technol. Lett.*, vol. 20, no. 10, pp. 767–769, May 2008.

[58] H. L. Lira, S. Manipatruni, and M. Lipson, "Broadband hitless silicon electro-optic switch for on-chip optical networks," *Opt. Exp.*, vol. 17, no. 25, pp. 22 271–22 280, 2009.

[59] B. G. Lee, A. Biberman, N. Sherwood-Droz, C. B. Poitras, M. Lipson, and K. Bergman, "High-speed 2×2 switch for multi-wavelength message routing in on-chip silicon photonic networks," presented at the Eur. Conf. Optical Communication, Brussels, Belgium, 2008.

[60] A. Biberman, N. Sherwood-Droz, B. G. Lee, M. Lipson, and K. Bergman, "Thermally active 4×4 non-blocking switch for networks-on-chip," in *Proc. IEEE 21st Annu. Meet. Lasers Electro-Optics Soc.*, 2008, pp. 370–371.

[61] A. W. Poon, F. Xu, and X. Luo, "Cascaded active silicon microresonator array cross-connect circuits for WDM networks-on-chip," *Proc. SPIE, Integr. Optoelectron. Devices*, vol. 6898, pp. 689 812-1–689 812-10, 2008.

[62] A. W. Poon, X. Luo, F. Xu, and H. Chen, "Cascaded microresonator-based matrix switch for silicon on-chip optical interconnection," *Proc. IEEE*, vol. 97, no. 7, pp. 1216–1238, Jul. 2009.

[63] A. Bianco, D. Cuda, R. Gaudino, G. Gavilanes, F. Neri, and M. Petracca, "Scalability of optical interconnects based on microring resonators," *IEEE Photon. Technol. Lett.*, vol. 22, no. 15, pp. 1081–1083, Aug. 2010.

[64] K. Yu, C.-H. Chen, A. Titriku, A. Shafik, M. Fiorentino, P. Y. Chiang, S. Palermo *et al.*, "25 Gb/s hybrid-integrated silicon photonic receiver with microring wavelength stabilization," in *Proc. Opt. Fiber Commun. Conf.*, Los Angeles, CA, USA, 2015, Paper W3A-6.

[65] Q. Xu, B. Schmidt, J. Shakya, and M. Lipson, "Cascaded silicon micro-ring modulators for WDM optical interconnection," *Opt. Exp.*, vol. 14, no. 20, pp. 9431–9435, 2006.

[66] H. Jayatilleka, M. Caverley, N. A. Jaeger, S. Shekhar, and L. Chrostowski, "Crosstalk limitations of microring-resonator based WDM demultiplexers on SOI," in *Proc. Opt. Interconnects Conf.*, Apr. 2015, pp. 48–49.

[67] N. Sherwood-Droz, K. Preston, J. S. Levy, and M. Lipson, "Device guidelines for WDM interconnects using silicon microring resonators," in *Proc. Workshop Interaction Between Nanophotonic Devices Syst. Located Micro*, 2010, vol. 43, pp. 15–18.

[68] B. A. Small, B. G. Lee, and K. Bergman, "On cascades of resonators for high-bandwidth integrated optical interconnection networks," *Opt. Exp.*, vol. 14, no. 22, pp. 10 811–10 818, 2006.

[69] M. Bahadori, D. Nikolova, S. Rumley, C. P. Chen, and K. Bergman, "Optimization of microring-based filters for dense WDM silicon photonic interconnects," in *Proc. Opt. Interconnects Conf.*, Apr. 2015, pp. 84–85.

[70] R. Hendry, D. Nikolova, S. Rumley, N. Ophir, and K. Bergman, "Physical layer analysis and modeling of silicon photonic WDM bus architectures," in *Proc. HiPEAC Workshop*, Jan. 2014, pp. 20–22.

[71] A. Biberman, P. Dong, B. G. Lee, J. D. Foster, M. Lipson, and K. Bergman, "Silicon microring resonator-based broadband comb switch for wavelength-parallel message routing," in *Proc. Laser Electro-Opt. Soc.*, 2007, pp. 474–475.

[72] B. G. Lee, B. A. Small, K. Bergman, Q. Xu, and M. Lipson, "Transmission of high-data-rate optical signals through a micrometer-scale silicon ring resonator," *Opt. Lett.*, vol. 31, no. 18, pp. 2701–2703, 2006.

[73] M. Georgas, J. Leu, B. Moss, C. Sun, and V. Stojanovic, "Addressing link-level design tradeoffs for integrated photonic interconnects," in *Proc. IEEE Custom Integr. Circuits Conf.*, 2011, pp. 1–8.

[74] N. Ophir, C. Mineo, D. Mountain, and K. Bergman, "Silicon photonic microring links for high-bandwidth-density, low-power chip I/O," *IEEE Micro*, vol. 33, no. 1, pp. 54–67, Jan./Feb. 2013.

[75] G. Masini, A. Narasimha, A. Mekis, B. Welch, C. Ogden, C. Bradbury, C. Sohn, D. Song, D. Martinez, D. Foltz *et al.*, "CMOS photonics for optical engines and interconnects," presented at the Optical Fiber Communication Conf., Los Angeles, CA, USA, 2012, Paper OTu2I-1.
[76] R. Wu, C.-H. Chen, J.-M. Fedeli, M. Fournier, R. Beausoleil, and K.-T. Cheng, "Compact modeling and system implications of microring modulators in nanophotonic interconnects," in *Proc. Int. Workshop Syst.-Level Interconnect Prediction*, 2015, pp. 1–6.
[77] C.-H. Chen, C. Li, R. Bai, K. Yu, J.-M. Fedeli, S. Meassoudene, M. Fournier, S. Menezo, P. Chiang, S. Palermo, M. Fiorentino, and R. Beausoleil, "DWDM silicon photonic transceivers for optical interconnect, in Optical Interconnects Conference," in *Proc. IEEE Opt. Interconnects Conf. (OI)*, 2015, pp. 52–53.
[78] A. Biberman, J. Chan, and K. Bergman, "On-chip optical interconnection network performance evaluation using power penalty metrics from silicon photonic modulators," in *Proc. IEEE Int. Interconnect Technol. Conf.*, 2010, pp. 1–3.
[79] Q. Li, D. Nikolova, D. Calhoun, Y. Liu, R. Ding, T. Baehr-Jones, M. Hochberg, and K. Bergman, "Single microring-based 2×2 silicon photonic crossbar switches," *IEEE Photon. Technol. Lett.*, vol. 27, no. 18, pp. 1981–1984, Sep. 2015.
[80] C.-H. Chen, M. A. Seyedi, M. Fiorentino, D. Livshits, A. Gubenko, S. Mikhrin, V. Mikhrin, and R. G. Beausoleil, "A comb laser-driven DWDM silicon photonic transmitter based on microring modulators," *Opt. Exp.*, vol. 23, no. 16, pp. 21 541–21 548, 2015.
[81] R. Hendry, D. Nikolova, S. Rumley, and K. Bergman, "Modeling and evaluation of chip-to-chip scale silicon photonic networks," in *Proc. IEEE 22nd Annu. Symp. High-Performance Interconnects*, 2014, pp. 1–8.
[82] J. G. Proakis, M. Salehi, N. Zhou, and X. Li, *Communication Systems Engineering*, vol. 1. Englewood Cliffs, NJ, USA: Prentice-Hall, 1994.
[83] E. Ip and J. M. Kahn, "Power spectra of return-to-zero optical signals," *J. Lightw. Technol.*, vol. 24, no. 3, pp. 1610–1618, Mar. 2006.
[84] R. Ramaswami, K. Sivarajan, and G. Sasaki, *Optical Networks: A Practical Perspective*. San Mateo, CA, USA: Morgan Kaufmann, 2009.
[85] J. D. Downie, "Relationship of Q penalty to eye-closure penalty for NRZ and RZ signals with signal-dependent noise," *J. Lightw. Technol.*, vol. 23, no. 6, pp. 2031–2038, Jun. 2005.
[86] K. Padmaraju, X. Zhu, L. Chen, M. Lipson, and K. Bergman, "Intermodulation crosstalk characteristics of WDM silicon microring modulators," *IEEE Photon. Technol. Lett.*, vol. 26, no. 14, pp. 1478–1481, Jul. 2014.
[87] A. Yariv, "Critical coupling and its control in optical waveguide-ring resonator systems," *IEEE Photon. Technol. Lett.*, vol. 14, no. 4, pp. 483–485, Apr. 2002.
[88] B. E. Little, S. T. Chu, H. A. Haus, J. Foresi, and J.-P. Laine, "Microring resonator channel dropping filters," *J. Lightw. Technol.*, vol. 15, no. 6, pp. 998–1005, Jun. 1997.
[89] H. Takahashi, K. Oda, and H. Toba, "Impact of crosstalk in an arrayed-waveguide multiplexer on N×N optical interconnection," *J. Lightw. Technol.*, vol. 14, no. 6, pp. 1097–1105, Jul. 1996.
[90] P. Dong, S. Liao, H. Liang, W. Qian, X. Wang, R. Shafiiha, D. Feng, G. Li, X. Zheng, A. V. Krishnamoorthy *et al.*, "High-speed and compact silicon modulator based on a racetrack resonator with a 1 V drive voltage," *Opt. Lett.*, vol. 35, no. 19, pp. 3246–3248, 2010.
[91] S. Assefa, F. Xia, W. M. Green, C. L. Schow, A. V. Rylyakov, and Y. Vlasov, "CMOS-integrated optical receivers for on-chip interconnects," *IEEE J. Select. Topics Quantum Electron.*, vol. 16, no. 5, pp. 1376–1385, Sep./Oct. 2010.
[92] J. E. Bowers, D. Dai, Y. Kang, and M. Morse, "High-gain high-sensitivity resonant Ge/Si APD photodetectors," *Proc. SPIE Defense, Security, Sensing*, vol. 7660, pp. 76 603H-1–76 603H-8, 2010.
[93] C. T. DeRose, D. C. Trotter, W. A. Zortman, A. L. Starbuck, M. Fisher, M. R. Watts, and P. S. Davids, "Ultra compact 45 GHz CMOS compatible germanium waveguide photodiode with low dark current," *Opt. Exp.*, vol. 19, no. 25, pp. 24 897–24 904, 2011.
[94] J. Proesel, A. Rylyakov, and C. Schow, "Optical receivers using DFE–IIR equalization," in *Proc. IEEE Int. Solid-State Circuits Conf. Dig. Tech. Papers*, 2013, pp. 130–131.
[95] M. H. Nazari and A. Emami-Neyestanak, "A 24-Gb/s double-sampling receiver for ultra-low-power optical communication," *IEEE J. Solid-State Circuits*, vol. 48, no. 2, pp. 344–357, Feb. 2013.

Meisam Bahadori received the B.Sc. degree in electrical engineering, majoring in communication systems, with honors and the M.Sc. degree in electrical engineering, majoring in microwaves and optics, both from the Sharif University of Technology, Tehran, Iran, in 2011, and June 2013. He joined the Lightwave Research Laboratory at Columbia University, New York, NY, USA, in fall 2014 where he is currently working toward the Ph.D. degree in electrical engineering with a focus on silicon photonics. From fall 2011 to spring 2014, he was a Research Assistant with the Integrated Photonics Laboratory, Sharif University of Technology. His current research interests include silicon photonic devices and nanophotonics.

Sébastien Rumley received the M.S. and Ph.D. degrees (in communication systems) from Ecole Polytechnique Fédérale de Lausanne, Lausanne, Switzerland, in 2005 and 2011, respectively, where he was a Research Assistant with the Telecommunications Laboratory between 2006 and 2011. He is currently an Associate Research Scientist at Columbia University, New York, NY, USA. His research interests include modeling and simulation of optical networks and interconnects, mainly for applications in high-performance computing and distributed computing platforms.

Dessislava Nikolova received the M.Sc. degree in solid-state physics from Sofia University, Sofia, Bulgaria, and the Ph.D. degree in computer science from the University of Antwerp, Antwerp, Belgium. She has spent two years as a Research Engineer in optical access networks with Alcatel working on scheduling algorithms for passive optical networks. After the Ph.D. degree, she received a Marie-Curie Fellowship to study the interaction between magnetism and plasmonics on the nanoscale at the London Center for Nanotechnology. Her current research interests include designing, modeling, and demonstrating silicon photonic systems for optical interconnects, switches, and quantum communication.

Keren Bergman (S'87–M'93–SM'07–F'09) received the B.S. degree from Bucknell University, Lewisburg, PA, USA, in 1988, and the M.S. and Ph.D. degrees from the Massachusetts Institute of Technology, Cambridge, MA, USA, in 1991 and 1994, respectively, all in electrical engineering. She is currently the Charles Batchelor Professor of electrical engineering at Columbia University, New York, NY, USA, where she is also the Scientific Director of the Columbia Nano Initiative. Her current research interests include optical interconnection networks for high-performance embedded computing, optical data center networks, and silicon photonic systems-on-chip.